Lukas Johann Görtschacher, BSc

Design and Development of an Antenna Transducer for a Backscatter RFID Sensor Tag

Master Thesis

Conducted for the purpose of receiving the academic title
Diplom-Ingenieur
in
Electrical Engineering

Submitted to
Graz University of Technology

Supervisor
Dipl.-Ing. Dr.techn. Jasmin Grosinger

Institute of Microwave and Photonic Engineering

Graz, October 2014

EIDESSTATTLICHE ERKLÄRUNG

Ich erkläre an Eides statt, dass ich die vorliegende Arbeit selbstständig verfasst, andere als die angegebenen Quellen/Hilfsmittel nicht benutzt und die den benutzten Quellen wörtlich und inhaltlich entnommenen Stellen als solche kenntlich gemacht habe.

Graz, am _____ _____

(Unterschrift)

Englische Fassung:

STATUTORY DECLARATION

I declare that I have authored this thesis independently, that I have not used other than the declared sources/resources and that I have explicitly marked all material which has been quoted either literally or by content from the used sources.

_____ _____

Date (Signature)

Danksagung

Ich möchte mich bei allen bedanken, die mich bei der Durchführung dieser Masterarbeit unterstützt haben.

Ein ganz besonderes Dankeschön an meine Eltern, Petra und Johann Görtschacher, die mich während des gesamten Studiums tatkräftig unterstützt haben.

Ganz besonders möchte ich mich auch bei Frau Dr. Jasmin Grosinger für die ausgezeichnete Betreuung bedanken. Sie hat mich in den wöchentlichen Treffen dem Ziel der erfolgreichen Durchführung dieser Masterarbeit durch wertvolle Ratschläge und Anregungen kontinuierlich näher gebracht und sich auch zusätzlich bei Bedarf stets Zeit genommen.

Lukas Görtschacher

Kurzfassung

Diese Masterarbeit beschäftigt sich mit dem Entwurf und der Entwicklung einer als Messumformer agierenden Antenne (Antennen-Transducer) für einen Sensor-Transponder, der bei 915 MHz betrieben wird. Dieser Sensor-Transponder wird im Weiteren in einem auf Signalrückstreuung basierenden Radio Frequency Identification-System (Backscatter RFID-System) eingesetzt. Der entwickelte Prototyp ist in der Lage drei verschiedene Wasserfüllstände zu detektieren und verfügt über leistungsstarke Umformer-Eigenschaften.
Ein Backscatter RFID-Sensor-System beruht auf der drahtlosen Kommunikation zwischen einem Lesegerät, welches als Kontrollsystem agiert, und einem Transponder, welcher sich aus der Messumformer-Antenne und einem Chip zusammensetzt. Die Identifikationsnummer und die Sensor-Informationen des Sensor-Transponders werden durch Modulation des rückgestreuten Signals zum Lesegerät übertragen. Der passive Chip des RFID-Sensor-Transponders wird durch das Hochfrequenzsignal des Lesegerätes mit Energie versorgt. Für eine zuverlässige und robuste Kommunikation zwischen dem Lesegerät und dem Transponder ist es wichtig, eine betriebssichere Energieversorgung des passiven Chips zu gewährleisten. Außerdem muss eine ausreichende Modulation des rückgestreuten Signals sichergestellt werden, welche eine korrekte Detektion der gesendeten Identifikationsnummer am Lesegerät ermöglicht.
In dieser Masterarbeit wird die Antenne des RFID-Sensor-Transponders als Messumformer verwendet um die Transponder-Umgebung aufzunehmen. Der Vorteil einer solchen Implementierung besteht darin, dass keine speziellen Sensor-Schnittstellen und Analog-Digital-Wandler im Transponder benötigt werden. Damit können bei dieser Implementierung standardisierte RFID-Chips verwendet werden.
Der in dieser Masterarbeit entworfene und umgesetzte Antennen-Transducer bildet die Sensor-Informationen auf die Phase des reflektierten Signals ab. Dieses Konzept der Phasen-Modulation hält die Leistungsübertragung zum Transponder-Chip konstant und gewährleistet damit im Vergleich zu bisher präsentierten Implementierungen eine zuverlässige Energieversorgung des

Chips. Zusätzlich besitzt der entwickelte Antennen-Transducer die positive Eigenschaft einer hohen Modulationseffizienz des Sensor-Transponders zur zuverlässigen Übertragung der Identifikationsnummer.

Abstract

This thesis deals with the design and the development of an antenna transducer for a backscatter radio frequency identification (RFID) sensor transponder (tag) operating at 915 MHz. The developed prototype is able to detect three different water filling levels and provides a high measured backscatter transducer performance.
A backscatter RFID sensor system relies on the wireless communication between a reader containing the control system and the tag consisting of the antenna transducer and a chip. The tag identification number (ID) and the sensing information are transmitted to the reader by modulating the backscattered signal. The passive chip of the RFID sensor tag is supplied by the radio frequency power sent from the reader. For a reliable and robust communication between the reader and the tag, it is vital to ensure a reliable power supply to the passive tag chip and to modulate the reflected backscatter signal in a way that it can be correctly detected at the reader.
In this work, the RFID sensor tag uses the antenna as transducing element to sense the tag environment. The benefit of such a sensor tag implementation is that no specific sensor interfaces and analog to digital converters are required. Also, off-the-shelf RFID chips can be used in such an implementation.
The designed and realized antenna transducer presented in this thesis maps the sensing information to the phase of the reflected signal. This phase modulation concept keeps the power transmission to the tag chip constant and thus ensures a reliable chip power supply in comparison to other realizations that have been presented so far. Additionally, the custom-built transducer prototype favorably ensures a high backscatter modulation efficiency for the tag ID transmission.

Contents

1 Introduction

In the late 1940's, first works were published exploring radio frequency identification (RFID), a technology as consequence of the development of radar [1].
As depicted in Figure 1.1, an RFID system consists of a reader and a transponder (tag) [2].
The commercial use of RFID started in the 1960's with the functionality that tags could be detected as present or absent. The commercial use of RFID for collecting tolls began in Europe in 1987 and raised in the 1990's. Nowadays, there are many applications for RFID and tags can be build out of a single antenna and a single chip, whereat the size of the tags is limited by the dimension of the antennas [1].
First functional passive ultra high frequency (UHF, 300 MHz - 3 GHz [3]) RFID systems appeared in the early 1970's [4].
In 2008, the concept of new passive UHF RFID tags were presented that provide sensing capabilities without any specific sensor interfaces and analog to digital converters (ADCs) [5]. An RFID system is called to be passive, if the tag is not supplied by an additional source in the tag, but by a radio frequency (RF) power received from the reader [2].
In the following, backscatter RFID systems and sensor tags are explained in more detail. Additionally, the motivation for this thesis, as well as the related work is presented in this chapter.

1.1 Backscatter RFID Systems

In backscatter RFID systems, the tag reflects the RF signal transmitted by the reader. To include information, the backscatter signal is reproducibly modulated by the tag.
A typical tag switches between its absorbing mode and reflecting mode to ensure this modulation. Figure 1.1 shows such a system, where the different modes are achieved by switching between two different complex

chip impedances $Z_{\text{Abs}} = R_{\text{Abs}} + jX_{\text{Abs}}$ and $Z_{\text{Ref}} = R_{\text{Ref}} + jX_{\text{Ref}}$. R denotes the real part of the impedance, while X denotes the imaginary part. The antenna is characterized by its complex impedance $Z_{\text{Ant}} = R_{\text{Ant}} + jX_{\text{Ant}}$ [2]. As can be seen in Figure 1.1, the radio link between the reader and the tag is divided into two links. Power and data are transmitted from the reader to the tag in the forward link, while the modulated backscatter signal is transferred in the backward link [6].
Limiting factors for the forward link (forward link limitations) are the chip sensitivity $P_{\text{Chip,min}}$ and the impedance match between the tag antenna and the tag chip. $P_{\text{Chip,min}}$ denotes the minimum RF power at the tag that is necessary to activate the chip. The impedance match between the antenna and the chip is described in Section 1.1.1 [4].
The limiting factors in the backward link (backward link limitations) are the reader receiver (RX) sensitivity $P_{\text{RX,Reader,min}}$ and the modulation efficiency η. $P_{\text{RX,Reader,min}}$ denotes the minimum backscattered power for a successful detection of the data [6]. The modulation efficiency η is described in Section 1.1.1.
Further limiting factors are the antenna characteristics of the reader and the tag (e.g. gain, polarization) and the propagation channel characteristics (e.g. path loss, fading). This factors are included in the transfer functions S_{21} (reader to tag) and S_{12} (tag to reader) of the radio channel [6].

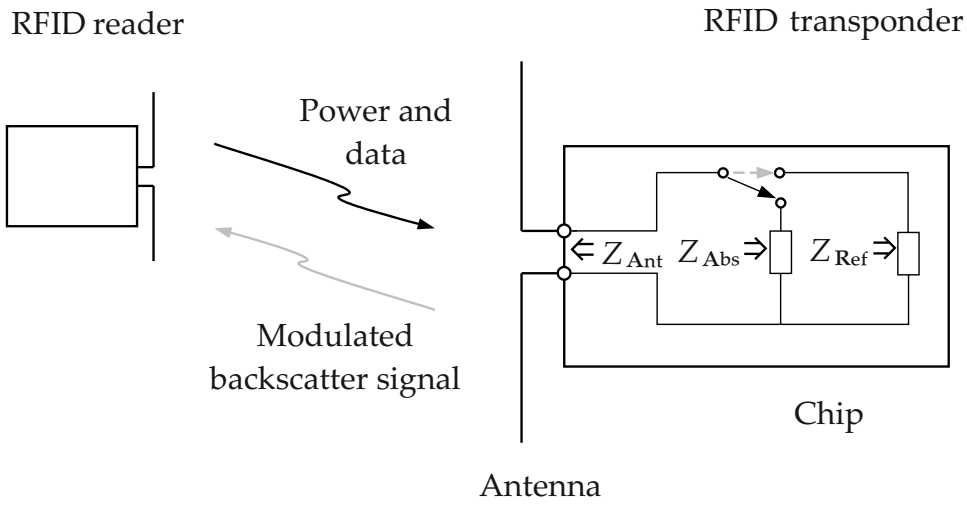

Figure 1.1: Backscatter RFID system [6]

1.1.1 Transponder

An RFID tag is depicted in Figure 1.1 on the right-hand side. As mentioned above, the reflected signal is modulated by switching between the chip absorbing impedance Z_{Abs} and the chip reflecting impedance Z_{Ref}. Typically, the amplitude is modulated by switching between the two modes and the tag identification number (ID) is transmitted that way [2]. The different chip impedances lead to different reflections at the input of the chip. In the following, this reflections are described by means of reflection coefficients.

Reflection Coefficient

The reflection coefficient S of a one-port network with complex load and source impedances Z_{L} and Z_{S} (see Figure 1.2) is defined as

$$S = \frac{Z_{\text{L}} - Z_{\text{S}}^*}{Z_{\text{L}} + Z_{\text{S}}}, \tag{1.1}$$

where Z_{S}^* is the complex conjugate impedance of Z_{S}. S is related to the reflected power at the load [7]. As can be seen from Equation 1.1, if the load impedance is matched to the source impedance ($Z_{\text{L}} = Z_{\text{S}}^*$), no reflections occur at the load ($S = 0$). If the load impedance is a short circuit ($Z_{\text{L}} = 0$) or an open circuit ($Z_{\text{L}} = \infty$), maximum reflections occur at the load ($|S| = 1$). Applying the previous definition to the backscatter RFID system in Figure 1.1, two different reflection coefficients S_{Abs} and S_{Ref} can be specified at the chip input for the two different tag modes (absorbing mode, reflecting mode) [6],

$$S_{\text{Abs}} = \frac{Z_{\text{Abs}} - Z_{\text{Ant}}^*}{Z_{\text{Abs}} + Z_{\text{Ant}}} \text{ and } S_{\text{Ref}} = \frac{Z_{\text{Ref}} - Z_{\text{Ant}}^*}{Z_{\text{Ref}} + Z_{\text{Ant}}}. \tag{1.2}$$

Power Transmission Coefficient

As mentioned above, the reflection coefficients S_{Abs} and S_{Ref} are related to the reflected power at the input of the chip. A measure for the transmitted power at the interface antenna/chip and hence an indication for the power available at the chip, P_{Chip}, is the power transmission coefficient τ that is defined as

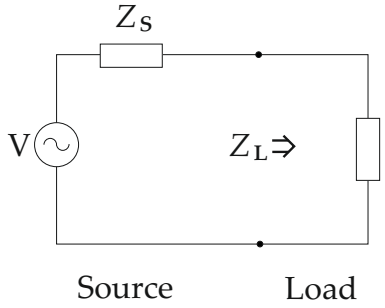

Figure 1.2: One-port network [7]: V is the source voltage.

$$\tau = 1 - |S_{\text{Abs}}|^2 = \frac{4R_{\text{Abs}}R_{\text{Ant}}}{|Z_{\text{Abs}} + Z_{\text{Ant}}|^2}. \tag{1.3}$$

τ lies between 0 and 1 that relates to no power transmission (open circuit, short circuit) and full power transmission (match), respectively [2], [8]. P_{Chip} can then be defined as

$$P_{\text{Chip}} = \tau |S_{21}|^2 P_{\text{TX,Reader}}, \tag{1.4}$$

where $P_{\text{TX,Reader}}$ is the power transmitted from the reader transmitter (TX) and $|S_{21}|^2$ is the channel gain of the forward link [6]. P_{Chip} must be larger than the chip sensitivity $P_{\text{Chip,min}}$ to activate the tag.

Modulation Efficiency

The modulation efficiency η describes the ability of distinction between the backscattered signals in the two different modes and is thus a measure for the modulation quality. It is defined as

$$\eta = \frac{2}{\pi^2} |S_{\text{Abs}} - S_{\text{Ref}}|^2 \tag{1.5}$$

and lies theoretically between 0 and a maximum of about 0.81 [9]. Typically, a maximum modulation efficiency of about 0.2 is realised (to ensure a large τ in the absorbing mode) [2].
The backscattered power received at the reader $P_{\text{RX,Reader}}$ can then be written as

$$P_{\text{RX,Reader}} = |S_{12}|^2 \eta |S_{21}|^2 P_{\text{TX,Reader}}, \tag{1.6}$$

with $|S_{12}|^2$ the channel gain of the backward link. $P_{\text{RX,Reader}}$ must be larger than the receiver sensitivity $P_{\text{RX,Reader,min}}$ for a correct interpretation of the tag information [6].

So far, the reflection coefficients S_{Abs} and S_{Ref}, the power transmission coefficient τ and the modulation efficiency η are presented in Section 1.1.1. Now, τ and η are applied to an exemplary constellation of the reflection coefficients S_{Abs} and S_{Ref}, denoted as constellation diagram, shown in Figure 1.3. As per Equation 1.3, $S_{\text{Abs}} = 0$ leads to $\tau = 1$ and $S_{\text{Ref}} = 1$ to $\tau = 0$. From Equation 1.5 it follows that a modulation efficiency of $\eta \approx 0.2$ is reached in this constellation.

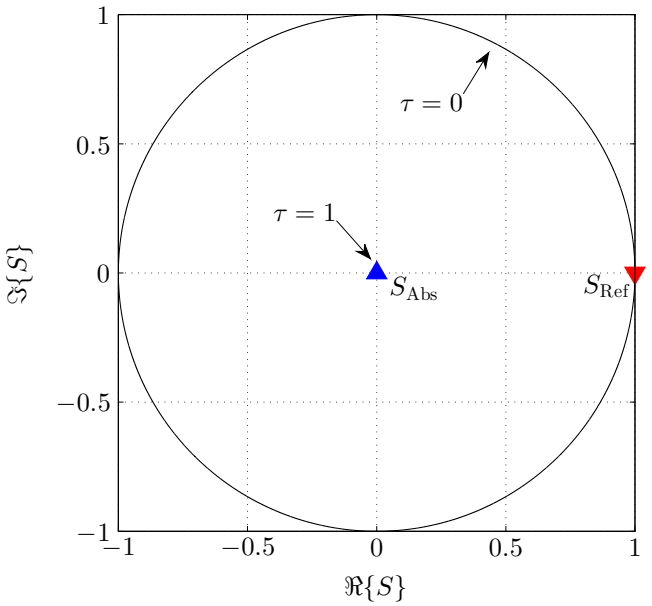

Figure 1.3: Real part $\Re\{S\}$ and imaginary part $\Im\{S\}$ of the tag reflection coefficients (Constellation diagram): $S_{\text{Abs}} = 0$, $S_{\text{Ref}} = 1$, and the corresponding τ-values are plotted.

1.1.2 Reader

A reader consists of a control system and an RF interface with a transmitter and a receiver [10]. As shown in Figure 1.1, the reader transmits power and data to the tag and receives the backscattered signal from the tag. A reader that is able to detect amplitude and phase information of the backscattered signal is presented by Angerer [11].

Baseband Signal Constellations at the Reader Receiver

Assuming a reader with one transmit and one receive antenna, backscattered signals at the reader RX can be modeled as described below [11].
After down conversion of the received signal, the baseband signal can be illustrated in the inphase and quadrature (I/Q) plane (exemplarily shown in Figure 1.4). L is the carrier leakage that mainly consists of the transmitted reader signal that leaks into the receive path of the reader [11]. In the absorbing mode, the tag absorbs the energy coming from the reader and the state $S^{(\mathrm{A})}$ can be detected at the reader RX. The state $S^{(\mathrm{R})}$ corresponding to the tag reflecting mode refers to the sum of the carrier leakage L and the tag signal h, $L + h$. h considers the channel transfer functions in both directions S_{21}, S_{12} and the reflection coefficients S_{Abs}, S_{Ref} (implies τ and η) of the tag [6]. To distinguish between the two states $S^{(\mathrm{A})}$ and $S^{(\mathrm{R})}$, the signals L and h have to be estimated by the RX of the reader [11].

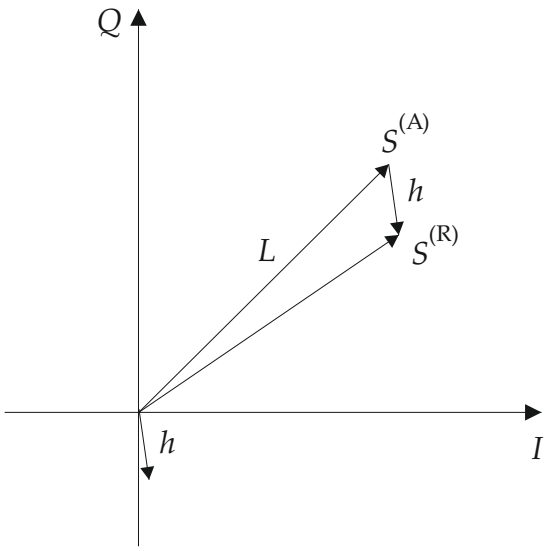

Figure 1.4: I/Q plane: Exemplary baseband signal constellation at the RFID reader RX with the two different states $S^{(A)}$ and $S^{(R)}$ [6].

1.2 RFID Sensor Tags

RFID sensor tags change their behavior with changes in the tag environment. To enable such a change of the sensor tag behavior, a transducer has to be integrated in the RFID tag. The transducer changes its impedance with changes in the tag environment and thus modulates the backscattered signal with the sensing information [2].
There are two types of transducers, namely an antenna transducer and a chip transducer. In the case of an antenna transducer, the tag antenna acts as transducing element and changes its input impedance Z_{Ant} with the environment change. An advantage of the antenna transducer is that an off-the-shelf chip can be used. In the case of a chip transducer, a transducing element is included in the chip itself. The transducer structure can be for example included in the chip reflecting impedance Z_{Ref} [6]. The advantage of this solution is that the absorbing impedance Z_{Abs} stays constant with respect to the changing environment. A constant Z_{Abs} implies a constant power transmission coefficient τ and thus assures a stable power supply to the chip (Equations 1.3 and 1.4). A disadvantage of this approach is that a custom-built chip has to be designed [6].

1.2.1 Antenna Transducer

The focus in this work lies on the design and realization of an antenna transducer due to the fact that an off-the-shelf chip can be used and the forward link limitations can be kept small with an intelligent antenna design.
Let Δ denote a specific state of the environment. The characteristic of an antenna transducer is to change its impedance with a change of the antenna surroundings or $Z_{\mathrm{Ant}} = f(\Delta) \Leftrightarrow Z_{\mathrm{Ant}}(\Delta)$. Figure 1.5 shows the schematic of a tag with an antenna transducer. The change of $Z_{\mathrm{Ant}}(\Delta)$ leads to a change of the reflection coefficients in absorbing and reflecting modes that are denoted as $S_{\mathrm{Abs}}(\Delta)$ and $S_{\mathrm{Ref}}(\Delta)$. This change again implies a dependence of the power transmission coefficient $\tau(\Delta)$ (Equation 1.3) and the modulation efficiency $\eta(\Delta)$ (Equation 1.5) on the environment.
A big design challenge in the case of an antenna transducer is to realize a high modulation efficiency $\eta(\Delta)$ for tag identification and a high power transmission coefficient $\tau(\Delta)$ for a sufficient power supply of the passive chip [6].
As mentioned above, the power transmission coefficient τ is a measure for the power available at the chip but also changes with the environment $\tau(\Delta)$. This fact makes it difficult to supply the chip with enough power at all different sensing states. The goal of this work is to design and realize an antenna transducer that overcomes this problem and ensures a reliable power supply to the chip.
The theoretical concept of that special kind of antenna transducer is introduced by Grosinger and Bösch [2]. The antenna changes its impedance in a way that the backscattered signal is phase modulated with the information about the environment (e.g., temperature, curvature, etc.) in the absorbing mode. The tag ID is still transmitted with the change between the absorbing mode and the reflecting mode. Due to the phase modulation, the amplitude of the absorbing reflection coefficient stays constant at the different sensing states of interest Δ_k ($k = 1...K$), so that $|S_{\mathrm{Abs}}(\Delta_k)| = \mathrm{const}$.
A reader that is able to detect amplitude and phase information of the backscattered signal is already presented in Section 1.1.2. This concept allows a detection of the sensor tag states that are provided with the presented antenna transducer.

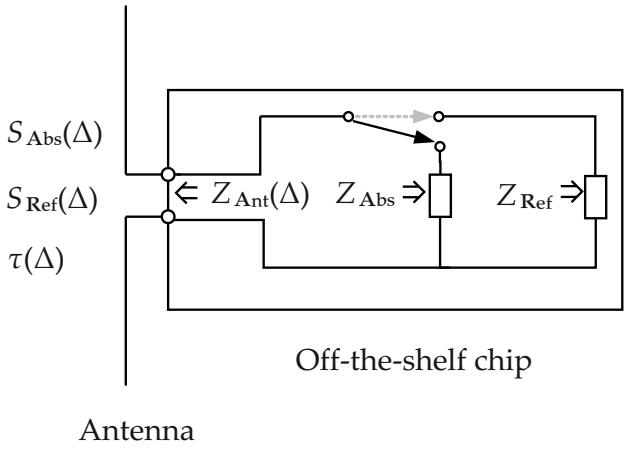

Figure 1.5: Sensor tag with antenna transducer [6]

1.2.2 Related Work

This section gives an overview about the related work that has been done so far in terms of antenna transducer sensor tags.

Liquid Level Sensing

An antenna transducer sensing the filling level of plastic boxes filled with low and high dielectrics is presented by Marrocco and Amato [12]. Single and multiple tags are attached vertically to boxes. The filling level is extracted from the measured backscattered power at the reader RX.
Attaching the antenna horizontally leads to a different possibility of fluid level sensing and is presented by Bhattacharyya *et al.* [13]. The tag is attached to a filled beverage glass and is thus influenced and detuned by the fluid inside. In case of an empty glass (or a specific threshold), the tag receives and reflects enough power to be detected by the reader. Therefore, a binary sensing is possible whether the glass is empty or not. An expansion of this binary approach is explored by Capdevila *et al.* [14], where multiple tags are attached vertically displaced to a container filled with water. The different tags response with their ID, if there is air and no liquid behind them, so that more discrete states can be sensed.
Similar approaches are done by Jiang *et al.* [15] for sensing liquid levels in medical transfusion applications. In contrast to the practices depicted above, where the transmitted power is constant, the parameter that is measured

to detect the sensing state is the transmitted power by the reader that is necessary to activate the tag.

Deformation Sensing

Besides the sensing of liquid levels there are tags able to sense deformation. Merilampi *et al.* [16] present a printed tag as wearable strain sensor that changes its dimension when stretched and thus the reflected signal power. Occhiuzzi *et al.* [17] present a sensor tag to sense deformation, where the sensing is accomplished by means of a meander line antenna. The antenna impedance is changed by a change of the antenna shape.
A sensor principle based on the degradation of the tag performance in the proximity of a metal is described by Bhattacharyya *et al.* [18]. The metal is attached to the monitored object, while a tag is placed in the near proximity. A deformation of the object changes the distance between the tag and the metal and thus detunes the tag.

Humidity and Moisture Sensing

Currently, humidity and moisture sensors are also discussed in the scientific community. For example, Gao *et al.* [19] investigate a printed coupling loop with a write-once-read-many sensor that is attached to an ordinary RFID tag. A humidity threshold event changes the impedance of the sensor and the coupling loop decreases the tag performance.
A folded patch tag as humidity sensor is presented by Manzari *et al.* [20]. A conducting polymer PEDOT:PSS is filled within the patch to realize a change in its electrical properties with a change in humidity. With this change, the properties of the tag are changed.

Temperature Sensing

Further sensor tags that are currently investigated are temperature sensors presented by Virtanen *et al.* [21] and Qiao *et al.* [22]. These sensors rely on the effect that water changes its relative permittivity ε as a function of temperature and thus changes the tag antenna characteristic when placed in the proximity of the tag.
A threshold heat sensor is introduced by Babar *et al.* [23], where paraffin

wax is used as sensing material. The wax irreversibly changes its characteristics with a certain temperature threshold and therefore detunes the tag permanently.
A mechanical thermal threshold sensor with shape-memory-alloy (SMA) is presented by Caizzone *et al.* [24]. The SMA is used as a switch. It mechanically deforms at a certain temperature and thus opens the switch at this threshold.

Gas Sensing

A gas sensor is published by Occhiuzzi *et al.* [25] that uses carbon nanotube (CNT) composites as transducer. The CNT composites absorb gas molecules and change their physical properties. This change influences the characteristics of the tag that can be measured at the reader.

Motion Sensing

Occhiuzzi *et al.* [26] present a motion sensor that is connected in series with a microchip. The sensor has two impedance states depending on the motion of a person (rest or movement). The tag is detuned at one state and thus cannot be detected by the reader.

In general, the antenna transducers presented so far map the sensor information to the amplitude of the backscattered signal. The detection of the information relies on the measurement of power, either on the received backscattered power or on the transmitted power at the reader that is necessary to activate the sensor tag. Both methods do not provide a constant power transmission to the tag. While the former suffers from that fact, the latter is based on it but requires a permanent adjustment of the transmitted power. The new concept with the presented antenna transducer maps the sensor information to the phase of the backscattered signal in the absorbing mode (see Section 1.2.1). Together with the reader that is presented in Section 1.1.2 a much more elegant detection mechanism can be applied. The main advantage of this concept is that the antenna transducer provides a constant amplitude in the absorbing mode and thus ensures a reliable power supply to the chip. Another advantage is that in general the tag ID can be detected more accurately [2].

2 Antenna Transducer

This chapter presents theoretical examinations of an antenna transducer for a passive RFID sensor tag that monitors water filling levels in plastic cans. The antenna transducer design should guarantee a reliable power supply to the passive tag chip. To assure this, a performance parameter is introduced that supports the selection of promising transducer designs and a fast evaluation of the developed prototypes. The aspired specifications are defined on the basis of an ideal antenna transducer.

2.1 Ideal Antenna Transducer

Figure 2.1 shows the constellation diagram of an ideal antenna transducer for four different sensing states Δ_1, Δ_2, Δ_3 and Δ_4 [2]. The ideal transducer is defined to ensure a high power transmission coefficient τ of 0.9 and a sufficient high modulation efficiency η at the four distinguishable sensing states Δ_k. Based on the constellation diagram of the ideal antenna transducer (see Figure 2.1), the following specifications for the design of the antenna transducer are aspired for this work.

- The antenna should be able to sense a minimum of two and a maximum of four different sensing states Δ_k ($k = 1...K$).
- The power transmission coefficient τ should be approximately 0.9.
- The center frequency (f_c) should lie between 860 MHz and 915 MHz.

For the tag antenna transducer design, no specific RFID chip is given. Therefore, the chip reflecting and absorbing impedances can be chosen freely. The chip absorbing impedance will be optimized in the following to reach a good sensor tag performance, while the chip reflecting impedance is assumed to be $Z_{\mathrm{Ref}} = (2 - \mathrm{j}0.1)\,\Omega$ [2]. Section 2.2.1 describes the procedure for the optimization of the chip absorbing impedance. Section 2.2.2 shows a way how to find appropriate antenna impedances if a special chip is used

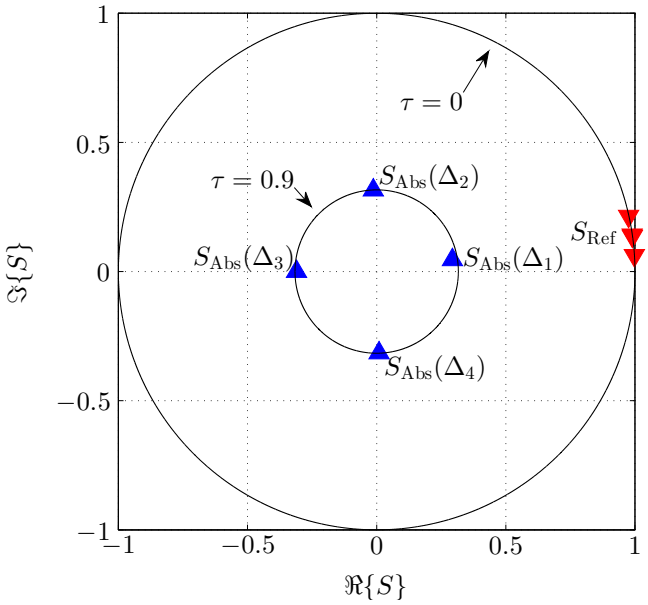

Figure 2.1: Constellation diagram of an ideal antenna transducer for four discrete sensing states Δ_1, Δ_2, Δ_3 and Δ_4: The corresponding reflection coefficients in the absorbing mode $S_{\mathrm{Abs}}(\Delta_1)$, $S_{\mathrm{Abs}}(\Delta_2)$, $S_{\mathrm{Abs}}(\Delta_3)$ and $S_{\mathrm{Abs}}(\Delta_4)$ lie on the $\tau = 0.9$-circle. The reflection coefficients in the reflecting mode S_{Ref} lie on the $\tau = 0$-circle [2].

with specific impedances. The latter is not used in this work but is very useful for further research.

2.2 Backscatter Transducer Efficiency

In order to assure an efficient antenna transducer design, a performance parameter α is introduced. This backscatter transducer efficiency, α, is defined as

$$\alpha = \left[\frac{\Delta\varphi_{\min}}{\frac{360^\circ}{K}} \left(1 - \frac{\max|\tau_{\text{ref}} - \tau|}{\beta} \right) \right]^{1/2} \tag{2.1}$$

under the condition that $|\tau_{\text{ref}} - \tau| \leq \beta$ and lies in the value range from 0 to 1. $\Delta\varphi_{\min}$ $\left(0 \leq \Delta\varphi_{\min} \leq {}^{360^\circ}/_{K}\right)$ is the minimum phase difference of the reflection coefficients $S_{\text{Abs}}(\Delta_k)$ in degrees, K $(2 \leq K \leq 4)$ is the number of discrete sensing states Δ_k, τ_{ref} is the reference value of τ that is per specification 0.9, and β $(0 \leq \beta \leq 0.9)$ is a weighting factor. Equation 2.1 can be rewritten as

$$\alpha = [\alpha_1 \cdot \alpha_2]^{1/2}, \tag{2.2}$$

where α is a function of α_1 that characterizes the phase differences of the absorbing reflection coefficients to each other and α_2 that gives a statement about the reflection coefficient amplitudes. In particular α_1 is an indicator for the phase configuration of the reflection coefficients and thus for the quality of the phase modulation. α_2 indicates the deviation of the power transmission coefficient τ from the reference value τ_{ref} and thus determines the power supply to the passive RFID chip. The weighting factor β is used to change the balance between α_1 and α_2 and thus the influence of $\Delta\varphi_{\min}$ and τ on the backscatter transducer efficiency α. An increasing β decreases the influence of τ on α, while the influence of the phase differences increases. Figures 2.2 and 2.3 show contour plots of α versus τ and $\Delta\varphi_{\min}$ for different values of β. From the figures it can be seen that a deviation of τ from τ_{ref} leads to a faster degradation of α in the case of $\beta = 0.1$ (Figure 2.3) than in the case of $\beta = 0.3$ (Figure 2.2). In the following, the default value of β is 0.3.

As stated above, α is defined as transducer performance parameter to give a quick reference of the quality of different antenna transducer designs. In case of the ideal antenna transducer presented in Figure 2.1 with $\Delta\varphi_{\min} = 83^\circ$, $\tau = 0.91$ [2] and $\beta = 0.3$, α reaches a high value of 0.94. For example, the maximum transducer efficiency of $\alpha = 1$ can be reached with $\Delta\varphi_{\min} = 90^\circ$ and $\tau = 0.9$ in the case of $K = 4$.

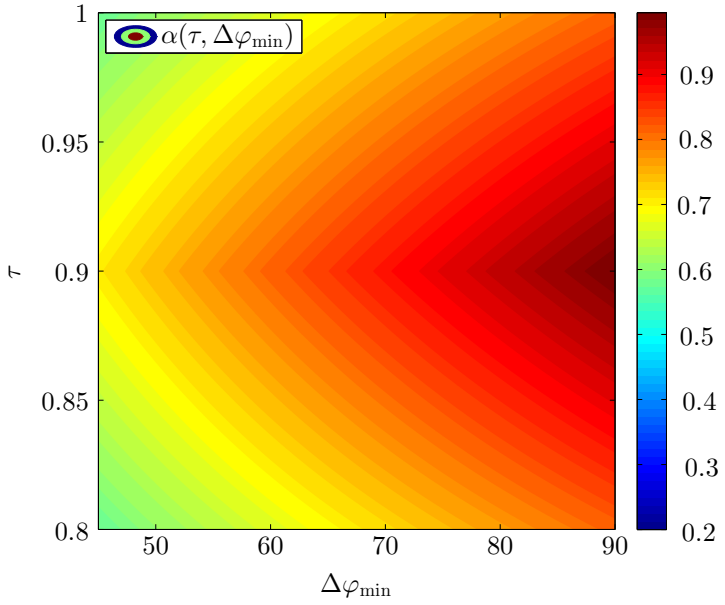

Figure 2.2: Contour plot of the backscatter transducer efficiency α for $\beta = 0.3$: α is plotted versus τ and $\Delta\varphi_{\min}$.

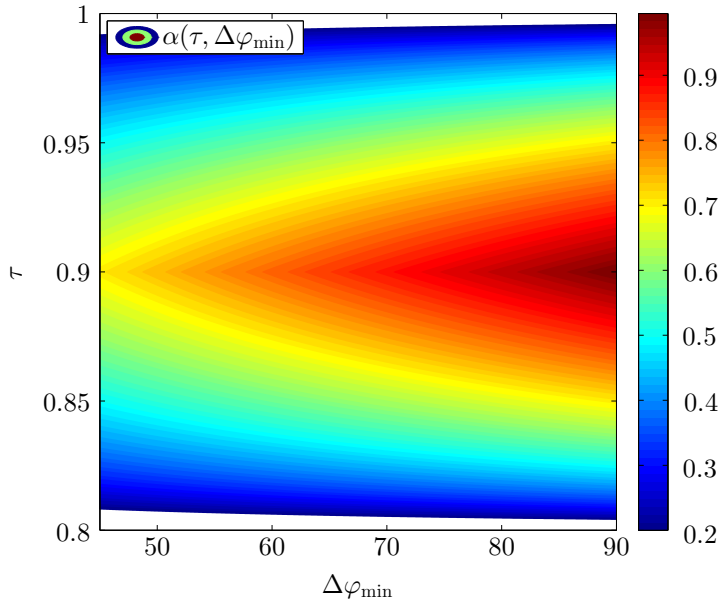

Figure 2.3: Contour plot of the backscatter transducer efficiency α for $\beta = 0.1$: In this case, the influence of τ on α is high. Only τ values close to the reference value $\tau_{\text{ref}} = 0.9$ lead to high α values.

2.2.1 Chip Impedance Optimization

In this section, the backscatter transducer efficiency α is used to find the optimal chip absorbing impedance in the case that the antenna impedances $Z_{\text{Ant}}(\Delta_k)$ at the different sensing states are known.
An algorithm is programmed within MATLAB [27] that automatically returns the optimal chip absorbing impedance. For this purpose, the reflection coefficients in absorbing mode $S_{\text{Abs}}(\Delta_k)$ are calculated with the known antenna impedances $Z_{\text{Ant}}(\Delta_k)$ and different possible absorbing impedances Z_{Abs} (see Equation 1.2). Each absorbing impedance Z_{Abs} leads to K absorbing reflection coefficients $S_{\text{Abs}}(\Delta_k)$ and the backscatter transducer efficiency α is calculated as per Equation 2.1. The absorbing impedance Z_{Abs} that causes the highest α-value is the optimal chip absorbing impedance.
Figure 2.4 shows this optimization graphically. A contour plot of backscatter transducer efficiency versus chip absorbing impedance is presented. The optimal chip absorbing impedance corresponds to the impedance where the backscatter transducer efficiency has a maximum. The used exemplary antenna transducer impedances are taken from Grosinger and Bösch [2] and are listed in Table 2.1. This choice allows a first verification of the algorithm because the optimized chip absorbing impedance can be directly compared to the published value. The optimal chip absorbing impedance is found to be $Z_{\text{Abs}} \approx (20 - \text{j}351)\,\Omega$ and matches with the published one [2]. Figure 2.5 shows the constellation diagram for the optimized absorbing impedance.

Sensing state	$Z_{\text{Ant}}(\Delta)\ (\Omega)$
Δ_1	$11 + \text{j}352$
Δ_2	$25 + \text{j}364$
Δ_3	$38 + \text{j}350$
Δ_4	$24 + \text{j}336$

Table 2.1: Antenna impedances Z_{Ant} of an antenna transducer at four sensing states [2]

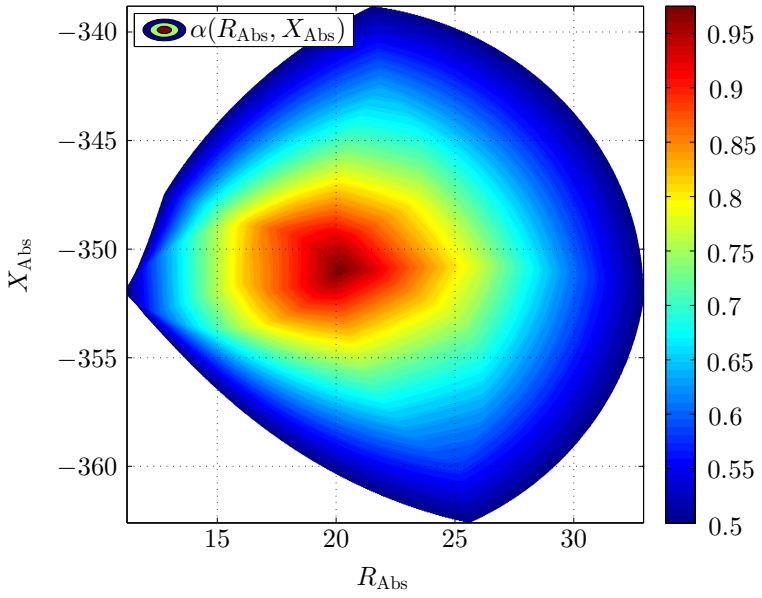

Figure 2.4: Contour plot of backscatter transducer efficiency α versus chip absorbing impedance $Z_{\mathrm{Abs}} = R_{\mathrm{Abs}} + jX_{\mathrm{Abs}}$ for given antenna impedances $Z_{\mathrm{Ant}}(\Delta_k)$ (see Table 2.1): The optimal chip absorbing impedance is $Z_{\mathrm{Abs}} \approx (20 - \mathrm{j}351)\,\Omega$. This value corresponds to the impedance where α has a maximum.

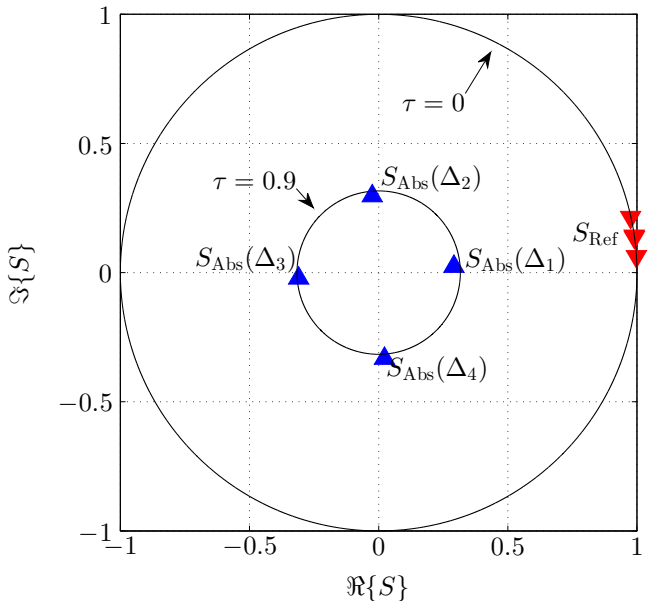

Figure 2.5: Constellation diagram with the optimal absorbing impedance $Z_{\mathrm{Abs}} \approx (20 - \mathrm{j}351)\,\Omega$ and antenna impedances $Z_{\mathrm{Ant}}(\Delta)$ as in Table 2.1: The reflection coefficients in the absorbing mode $S_{\mathrm{Abs}}(\Delta_k)$ have approximately 90° phase difference to each other and lie close to the $\tau = 0.9$-circle.

2.2.2 Antenna Impedance Optimization

Another possibility for the use of α is to find appropriate antenna impedances $Z_{\mathrm{Ant}}(\Delta_k)$ for a given chip absorbing impedance Z_{Abs}. In this section, an absorbing impedance of $Z_{\mathrm{Abs}} = (20 - \mathrm{j}350)\,\Omega$ is assumed.
In order to find rules for optimal antenna transducer impedances, the parameter α is presented as $\alpha = \sqrt{\alpha_1 \alpha_2}$, where α_1 only depends on the minimum phase difference $\Delta\varphi_{\mathrm{min}}$ and α_2 on the power transmission coefficient τ (see Equation 2.2). An implemented MATLAB program generates plots that illustrate α_1 and α_2 versus antenna impedance Z_{Ant} for the given chip absorbing impedance. The input parameters for this code are Z_{Abs}, τ_{Ref}, K, and one arbitrary reflection coefficient phase $\varphi_{\mathrm{Abs}}(\Delta_{\mathrm{init}})$[1] (init $\in [1, K]$).
Figure 2.6 shows a contour plot of α_1 versus antenna impedance for four sensing states ($K = 4$). Four regions of optimal R_{Ant} and X_{Ant} can be immediately identified in the figure. Choosing antenna impedances out of these high α_1-region leads to a good phase modulation behavior of the antenna transducer.
Figure 2.7 presents regions where antenna impedances Z_{Ant} can be found that ensure small deviations from the reference value τ_{Ref}. The constant α_2-regions lead to constant τ-circles in the constellation diagrams (see e.g. Figure 2.5), especially $\alpha_2 = 1$ leads to $\tau = 0.9$.
Combining α_1 and α_2 to the joint parameter α creates the contour plot shown in Figure 2.8. Optimal antenna impedances can be directly extracted from the plot. Here, the chosen absorbing impedance makes it possible to verify the algorithm. $Z_{\mathrm{Abs}} = (20 - \mathrm{j}350)\,\Omega$ and the antenna impedances in Table 2.1 are used for the constellation diagram of the ideal antenna transducer in Figure 2.1. So, the optimal antenna impedances from Figure 2.8 can be directly compared to the antenna impedances listed in Table 2.1.
The parameters Z_{Abs}, $\varphi_{\mathrm{Abs}}(\Delta_{\mathrm{init}})$, τ_{Ref}, and the amount of sensing states K can be easily changed, in order to fulfill different specifications. This fact makes the programmed MATLAB code an effective tool. Figure 2.9 shows a scenario with three discrete sensing states.

[1] One angle has to be fixed, otherwise there would be an infinite number of possible solutions.

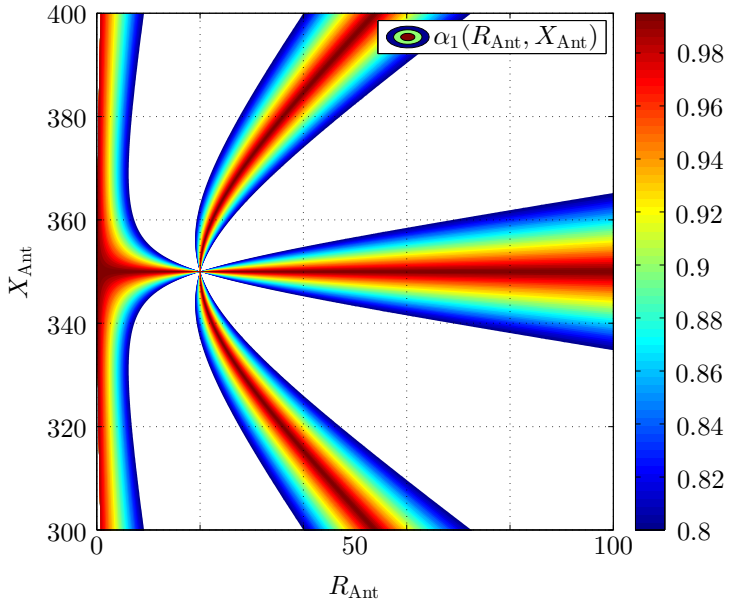

Figure 2.6: Contour plot of α_1 versus antenna impedance Z_{Ant}: α_1 is an indicator for the quality of the implemented phase modulation. Four regions can be distinguished. Each region stands for one sensing state. If the changing antenna impedance lies in different high α_1-regions for all sensing states, a good phase modulation is guaranteed.

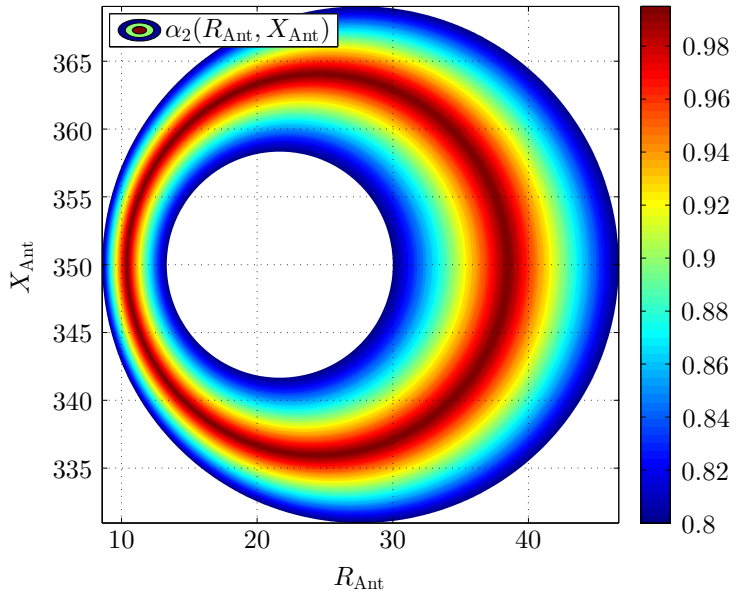

Figure 2.7: Contour plot of α_2 versus antenna impedance Z_{Ant}: α_2 is an indicator for the power transmission. If the antenna impedances lie in high α_2-regions for all sensing states, a small deviation of τ to τ_{Ref} is guaranteed.

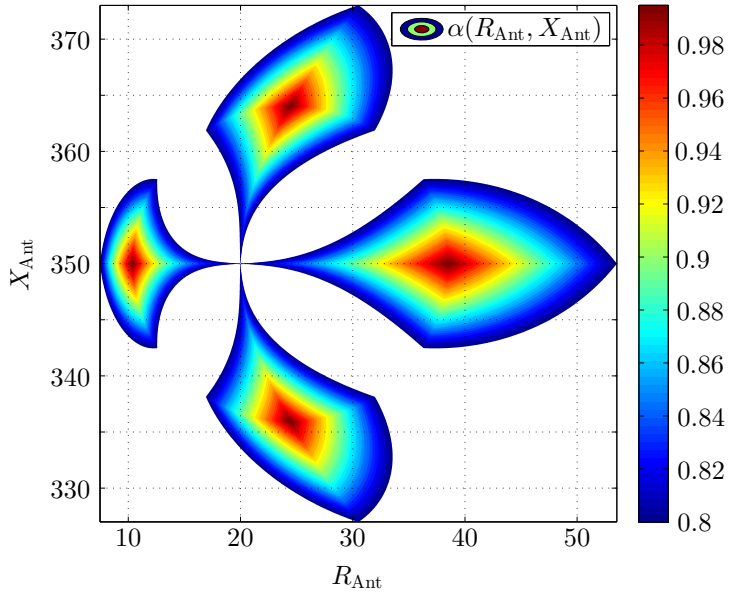

Figure 2.8: Backscatter transducer efficiency α versus Z_{Ant} for four sensing states for $Z_{\mathrm{Abs}} = (20 - \mathrm{j}350)\,\Omega$ and $\varphi_{\mathrm{Abs}}(\Delta_1) = 0°$: If the antenna impedances are chosen from the high α-regions for the different sensing states, a high backscatter transducer efficiency is guaranteed.

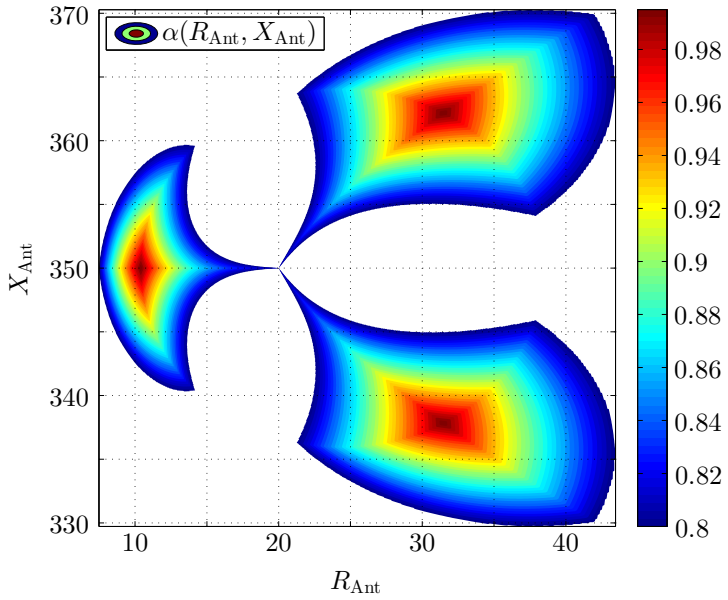

Figure 2.9: Backscatter transducer efficiency α versus Z_{Ant} for three sensing states for $Z_{\mathrm{Abs}} = (20 - \mathrm{j}350)\,\Omega$ and $\varphi_{\mathrm{Abs}}(\Delta_1) = 0°$: Three regions can be distinguished in this case.

3 Transducer Design and Prototype

The previous chapter defines the specifications for the antenna transducer for a passive RFID sensor tag that monitors water filling levels. The performance parameter α has been introduced to evaluate the performance of various transducer designs and prototypes. Two optimization algorithms has been presented in the Sections 2.2.1 and 2.2.2 that are based on α.
This chapter presents the antenna transducer design, the prototype, and the input impedance measurement of the latter. The measurement setup and the calibration of the measurement are also presented in this chapter. The measurements verify that the presented antenna transducer prototype is able to sense three discrete sensing states at a center frequency of $f_c = 915\,\text{MHz}$.

3.1 Transducer Design

Starting point of the antenna transducer design is a T-matched dipole antenna (see Figure 3.1) that promises to be a suitable structure to act as an antenna transducer [2]. Figure 3.2 shows the T-matched dipole in the schematic setup of the sensing scenario. The antenna, which is mounted on a substrate, is attached vertically to a plastic can and the 0 mm-level of the water is assumed to be in the middle of the dipole feed. The chosen substrate is AR1000 from ARLON [28] with a thickness of 0.8 mm. The can consists of a 1 mm thick PE-HD material [29].
Depending on the filling level of the can, the antenna should change its input impedance Z_{Ant} in a proper way. Thus, the sensing scenario is simulated within CST MICROWAVE STUDIO [30]. The shape of the T-matched dipole is changed for each simulation pass to find a proper transducer design. The geometry of the transducer that is used in the simulations and its design parameters can be seen in Figure 3.1.

The antenna transducer is simulated within a frequency range of 500 MHz to 3 GHz at the different filling levels. The antenna input impedances are exported for the frequency range of 860 MHz to 915 MHz from CST MICROWAVE STUDIO and imported into MATLAB for further evaluation. This evaluation includes the chip impedance optimization (see Section 2.2.1) and the following rating of the backscatter transducer efficiency α. From the high number of parameters, it can be seen that there are many possible antenna configurations. Additionally, a sweep of the water filling level has to be done for each configuration.
The final geometry parameters of the prototype found through simulations are listed in Table 3.1. The dimension of the substrate is 90 mm x 33 mm.

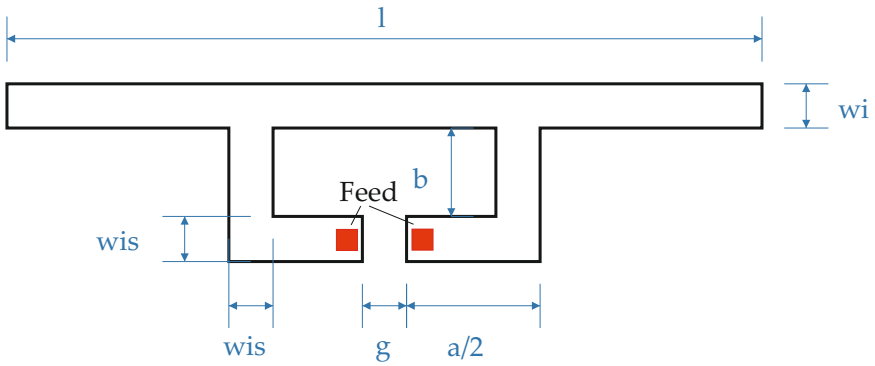

Figure 3.1: T-matched dipole with its geometry parameters

Geometry parameter	length (mm)
l	17
b	6
a	2
g	80
wi	12
wis	5

Table 3.1: Geometry parameters of the antenna transducer

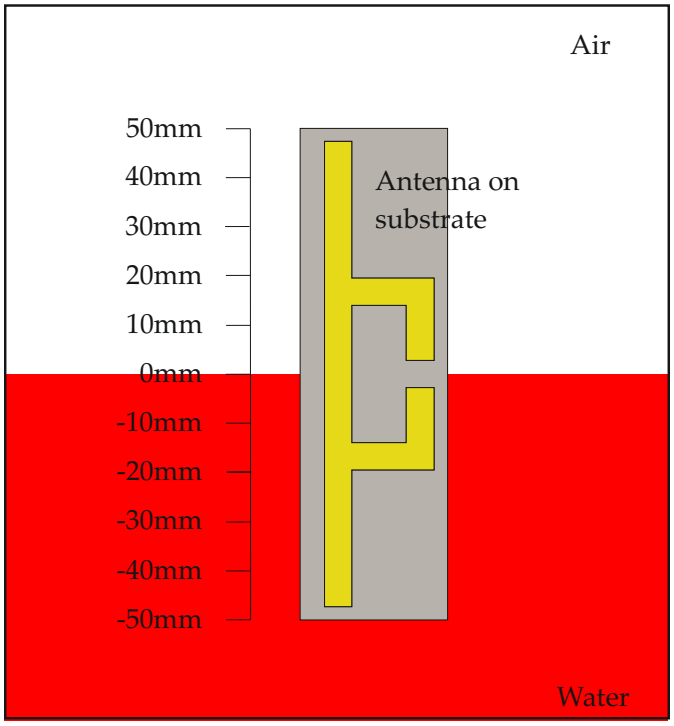

Figure 3.2: Schematic setup of the sensing scenario: The antenna on the substrate is attached to a can filled with water. The 0mm-level is in the middle of the dipole feed.

3.2 Prototype

Figure 3.5 shows a prototype that is realized based on the design presented in Section 3.1 (see Figure 3.1 and Table 3.1). Figure 3.3 shows the constellation diagram of the simulated antenna transducer prototype for an optimized chip absorbing impedance of $Z_{\text{Abs}} = (13 - \text{j}101)\,\Omega$. The constellation diagram shows three different sensing states ($-20\,\text{mm}$, $5\,\text{mm}$ and $40\,\text{mm}$) at $f_c = 915\,\text{MHz}$. This constellation leads to a backscatter transducer efficiency of $\alpha = 0.88$ with $\Delta\varphi_{\text{min}} = 101^\circ$ and with a maximum deviation from the τ-reference value of 0.027 which corresponds to about 3 %. The sensing states and the corresponding parameters, namely the antenna impedance Z_{Ant}, the power transmission coefficient τ, the modulation efficiency η, and the phase of the absorbing reflection coefficient φ_{Abs} are listed in Table 3.2. An efficient antenna transducer that is able to detect four sensing states could not be found for this prototype. The lower bound of the backscatter transducer efficiency α is defined to be 0.77 in this work and could not be

realized for a four sensing state scenario. The upper bound of α is due to the upper bounds of α_1 and α_2 that are defined to be 0.7 and 0.85 respectively (see Equation 2.2). This leads to a minimum $\Delta\varphi_{\text{min}}$ of 84° for a three sensing state scenario and to 63° for a four sensing state scenario. The resulting maximum tolerable deviation of τ from τ_{ref} is 0.045 for both scenarios.

Filling level (mm)	Z_{Ant} (Ω)	τ	η	φ_{Abs} (°)
$\Delta_1 = -20$	$6.6 + \text{j}98.4$	0.873	0.09	-14
$\Delta_2 = 5$	$19.6 + \text{j}111.6$	0.873	0.21	104
$\Delta_3 = 40$	$23.2 + \text{j}97.5$	0.916	0.33	-155

Table 3.2: Water filling levels and corresponding parameters of the simulated antenna transducer prototype for an optimized chip absorbing impedance of $Z_{\text{Abs}} = (13 - \text{j}101)\,\Omega$ at 915 MHz: Antenna impedance Z_{Ant}, power transmission coefficient τ, modulation efficiency η, and phase of the absorbing reflection coefficient φ_{Abs} at 915 MHz

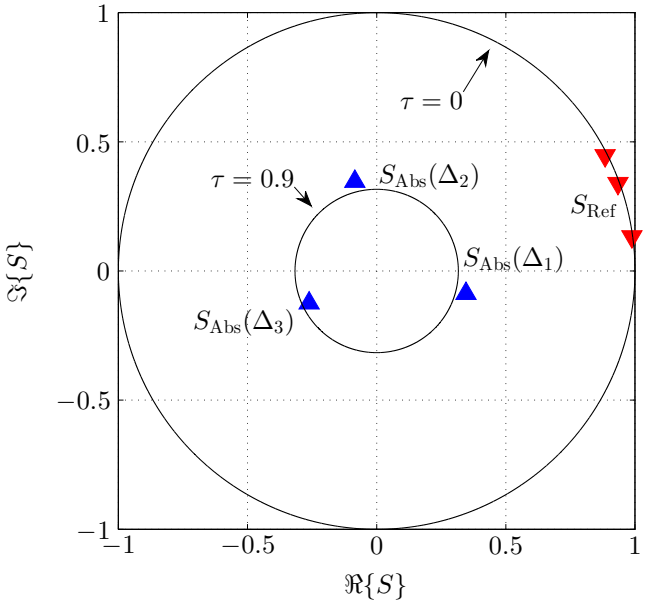

Figure 3.3: Constellation diagram of the simulated antenna transducer prototype for an optimized chip absorbing impedance of $Z_{\text{Abs}} = (13 - \text{j}101)\,\Omega$ at 915 MHz: This constellation leads to a backscatter transducer efficiency of $\alpha = 0.88$.

3.2.1 Impedance Measurement Setup

This section shows the setup for the impedance measurement of the prototype presented above. The used measurement setup is depicted in Figure 3.4 and was initially presented by Grosinger *et al.* [31].
A vector network analyzer (VNA) from type R&S ZVA67 is used to measure the reflection coefficient at the input of the antenna. The true differential mode of the VNA provides a symmetric feed of the antenna. An unsymmetric feed would lead to common mode currents that cause radiation and change the antenna properties [31]. In order to connect the antenna to the cables of the VNA, a test fixture has to be used. Figure 3.5 shows the T-matched dipole on the AR1000 substrate with a thickness of 0.8 mm, and the test fixture that is soldered to the T-feed of the antenna. The latter consists of miniature coaxial connectors (U.FL series by Hirose Electric Co. LTD.) and copper lines etched on a FR-4 substrate with 1.6 mm thickness. The measurement setup with the antenna mounted on the can can be seen in Figures 3.9 and 3.10. The coaxial cables are connected to the test fixture and are mechanically stabilized by a heat shrink tube. The thin coaxial cables with U.FL connectors are connected to the thick coaxial cables with SMA connectors with an adapter from RS Components [32]. The thick coaxial cables are connected to two physical ports of the VNA.

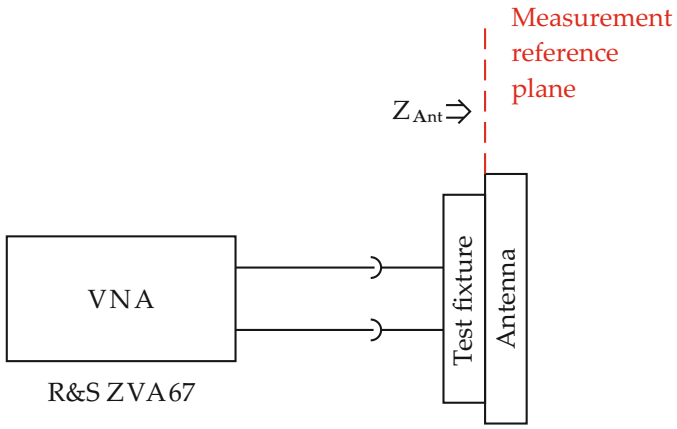

Figure 3.4: Antenna impedance measurement setup [31]

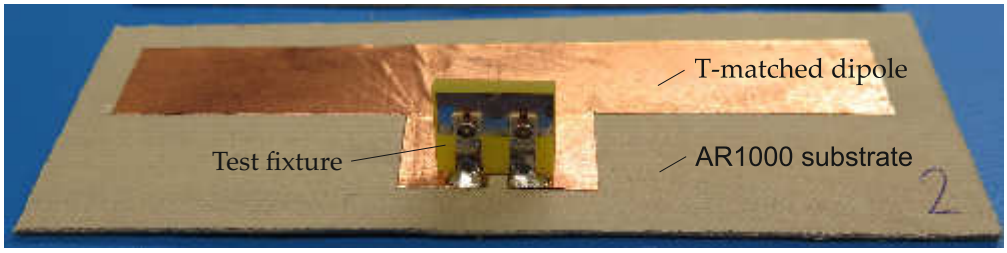

Figure 3.5: T-matched dipole on the AR1000 substrate: The test fixture is soldered on the T-feed of the dipole.

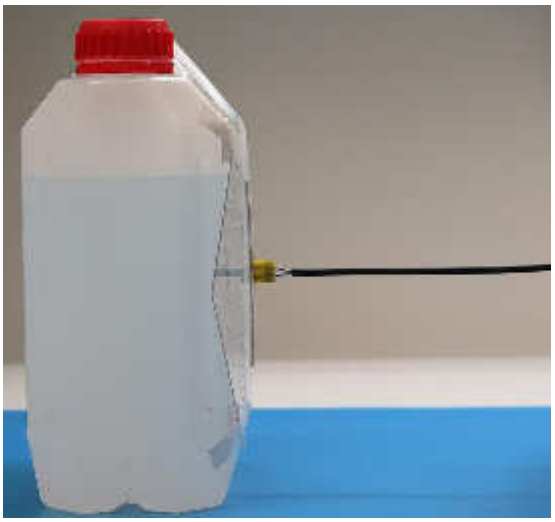

Figure 3.6: Measurement setup: The antenna with its measurement cables is mounted on the can filled with water.

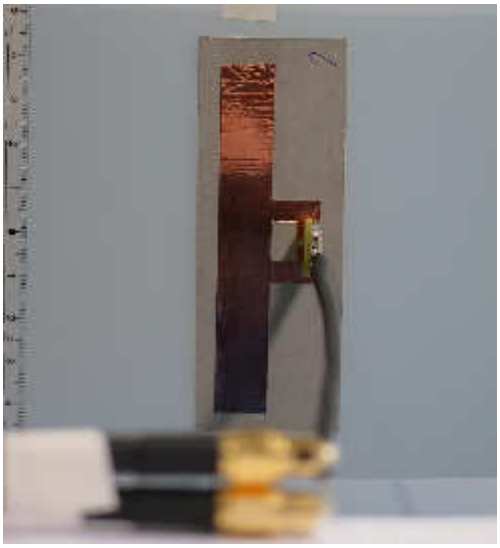

Figure 3.7: Measurement setup: The coaxial cables are fixed with a heat shrink tube. SMA connectors and U.FL connectors are connected via an adapter from RS Components [32] (can be seen in the front of the picture).

To shift the measurement reference plane to the input of the antenna, a calibration is necessary [33]. The calibration eliminates systematic errors in the measurement results that are introduced by cables, adapters, the test fixture, and the VNA itself. A calibration of the logical port in the differential mode requires a two-port calibration of the two physical ports. A calibration type that promises high accuracy consists of the four standards: open, short, match, and through standards [33]. The custom-built calibration kit used in this work is shown in Figure 3.8 [31]. Figure 3.8 shows the calibration kit (FR-4, 1.6 mm) and Table 3.3 lists the resistance R of the defined standards.

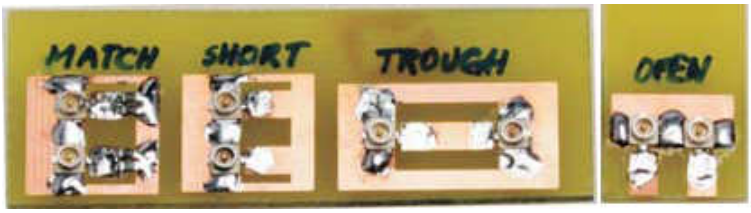

Figure 3.8: Custom-built calibration kit: The standards are mounted on FR-4 substrate of 1.6 mm thickness [31].

Standard	R (Ω)
Open	∞
Short	0
Match	50
Through	0

Table 3.3: Definition of the calibration standards [31]

For a verification of the measurement setup and the calibration, a dipole without a t-matched feed (test dipole) is measured on 1.6 mm FR-4 substrate and compared with simulations. The dimensions of the test dipole are depicted in Figure 3.9. Figure 3.10 shows the measured and simulated antenna impedances over the frequency. It can be seen that the simulations and the measurement results agree well. Thus, the measurement setup and the calibration are assumed to be accurate.

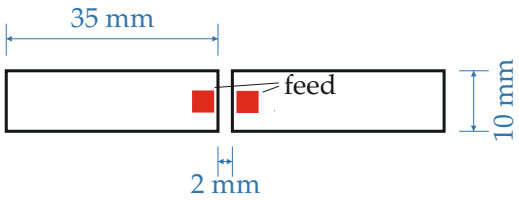

Figure 3.9: Dimensions of the test dipole that is used for verification of the measurement setup

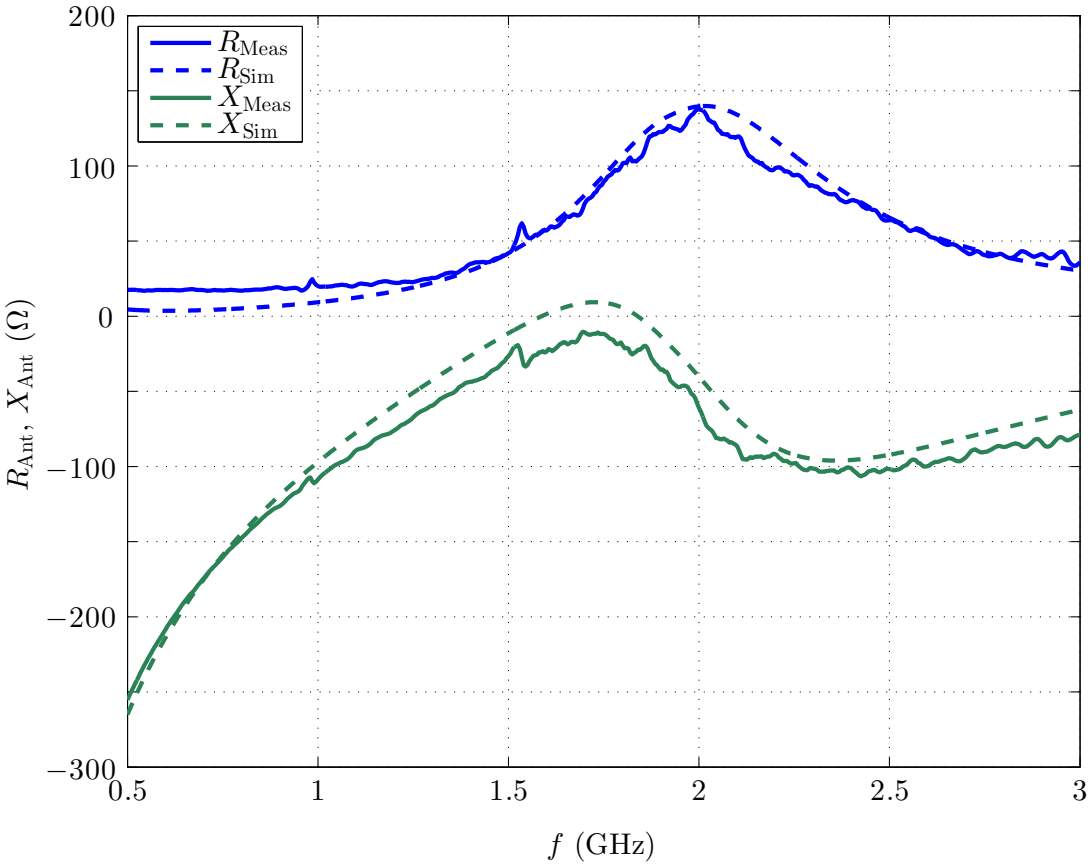

Figure 3.10: Real part R_{Ant} and imaginary part X_{Ant} of the test-dipole impedance for verification of the measurement setup

3.2.2 Measurement Results

The presented measurement results are averaged with a factor of 5 to eliminate random errors. 5 consecutive sweeps are averaged automatically

by the VNA. Figures 3.11 and 3.12 show the antenna behavior as a function of the water filling levels in the frequency range of 850 MHz to 950 MHz. The antenna resistance R_{Ant} and the antenna reactance X_{Ant} are plotted at several water filling levels.

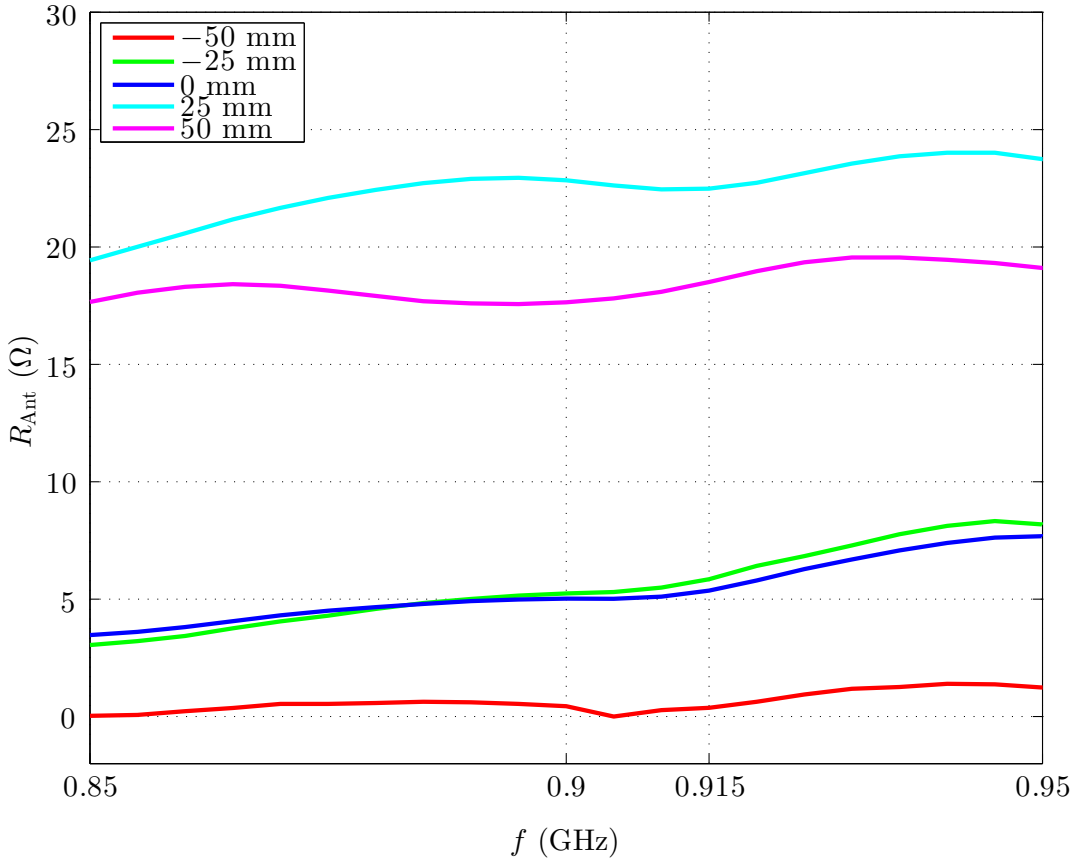

Figure 3.11: Antenna resistance R_{Ant} versus frequency f: Series of different water filling levels in 25 mm steps are plotted.

The measured antenna impedances at the sensing states −20 mm, 5 mm and 40 mm are shown for a frequency range of 500 MHz to 3 GHz in Figures 3.13, 3.14 and 3.15. The measured resistance R_{Ant} and the reactance X_{Ant} of the antenna are compared to the simulated results. In contrast to the verification measurement shown in Figure 3.10, higher differences can be observed between the measurement and the simulations, but the behavior of the measured and the simulated transducer over the water level is the same. On the one hand, the differences can be explained by the not lifelike

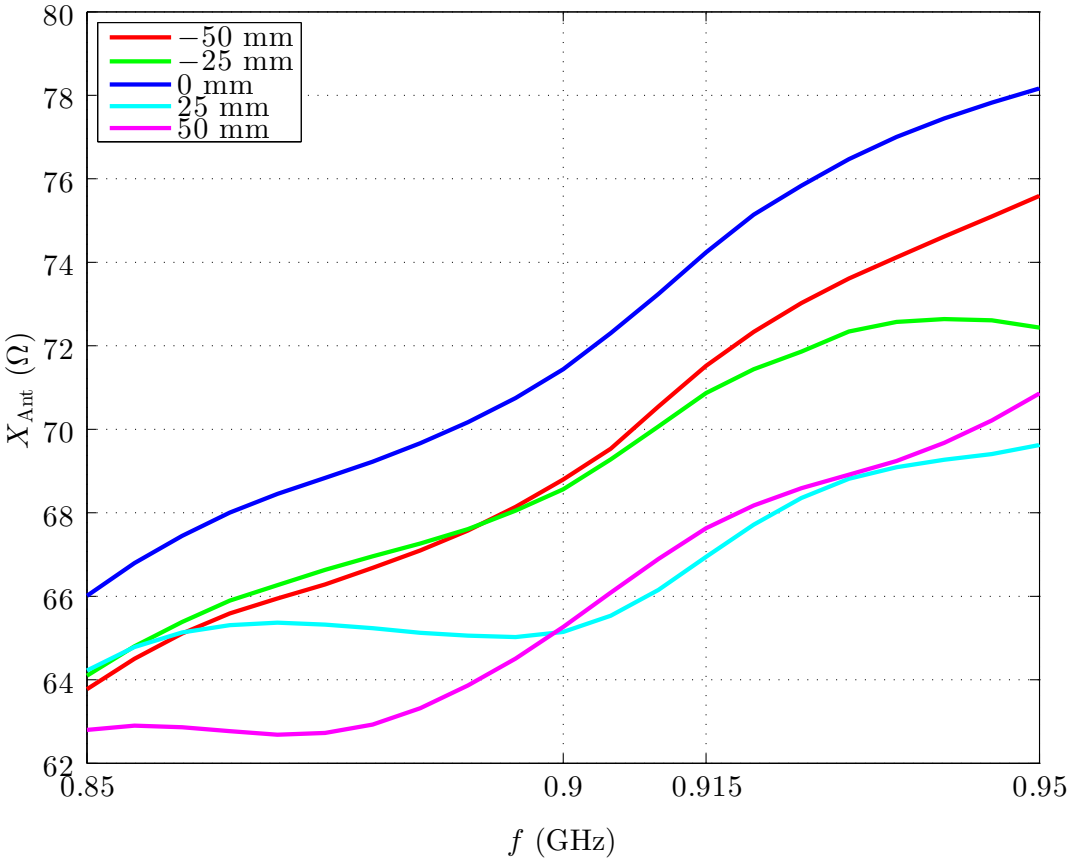

Figure 3.12: Antenna reactance X_{Ant} versus frequency f: Series of different water filling levels in 25 mm steps are plotted.

reproduction of the setup in the simulations (deviation of dimensions, material parameters, et cetera). On the other hand, the influence of test fixture on the complex feeding structure of the T-matched antenna distorts the measurement results. The influence of the test fixture has been decreased, but not eliminated with the use of the substrate. The substrate increases the measurement accuracy at water levels lower than 0 mm. At water levels above 0 mm the high relative permittivity of the water itself ($\epsilon_r \approx 80$) decreases the influence of the test fixture on the measurement results. The used AR1000 substrate is 0.8 mm thick an has a relative permittivity of $\epsilon_r \approx 10$, which is higher than that of FR-4 ($\epsilon_r \approx 4.3$), but much smaller than that of water.

To show the reproducibility of the measurement, a second sample of the antenna transducer (R_{Ver}, X_{Ver}) is measured. An exemplary measurement

series at the water filling level of 40 mm is shown in Figure 3.16. The differences can be explained by the slightly variation of the two samples caused by the manufacturing process.

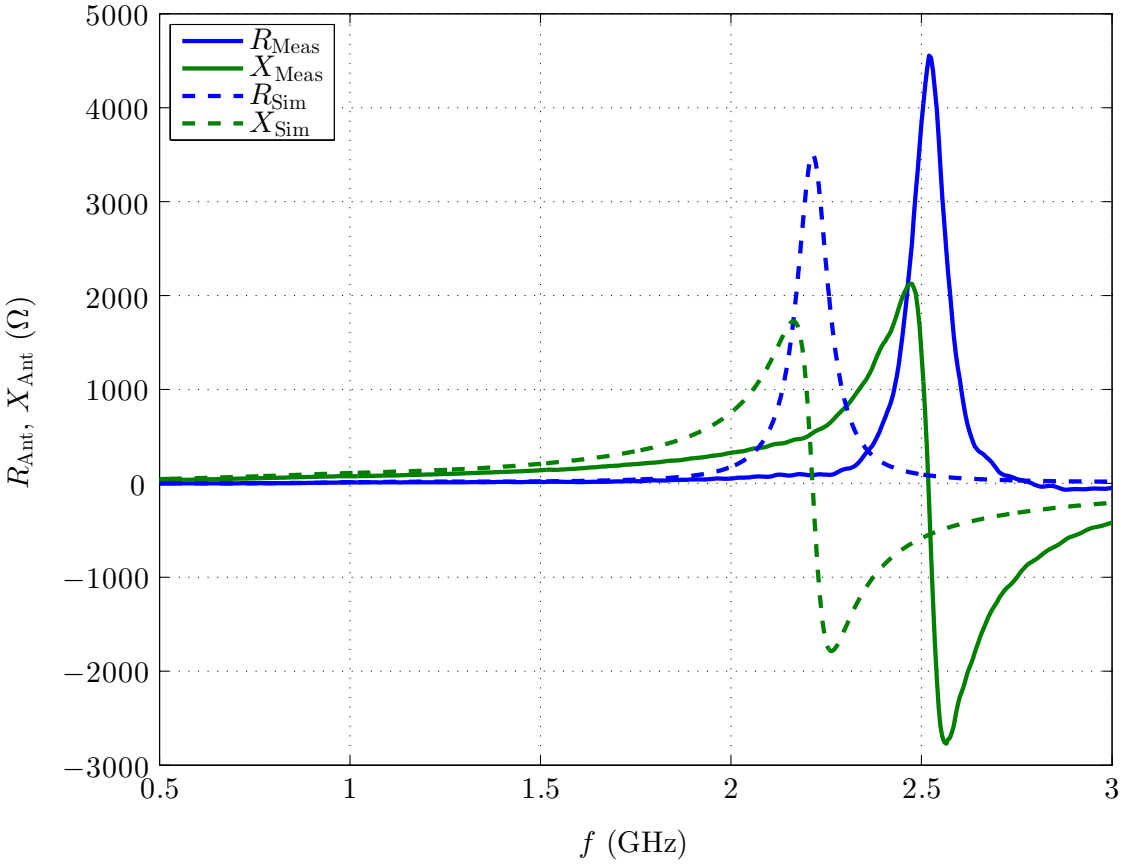

Figure 3.13: Antenna resistance R_{Ant} and reactance X_{Ant} versus frequency f at -20 mm water filling level

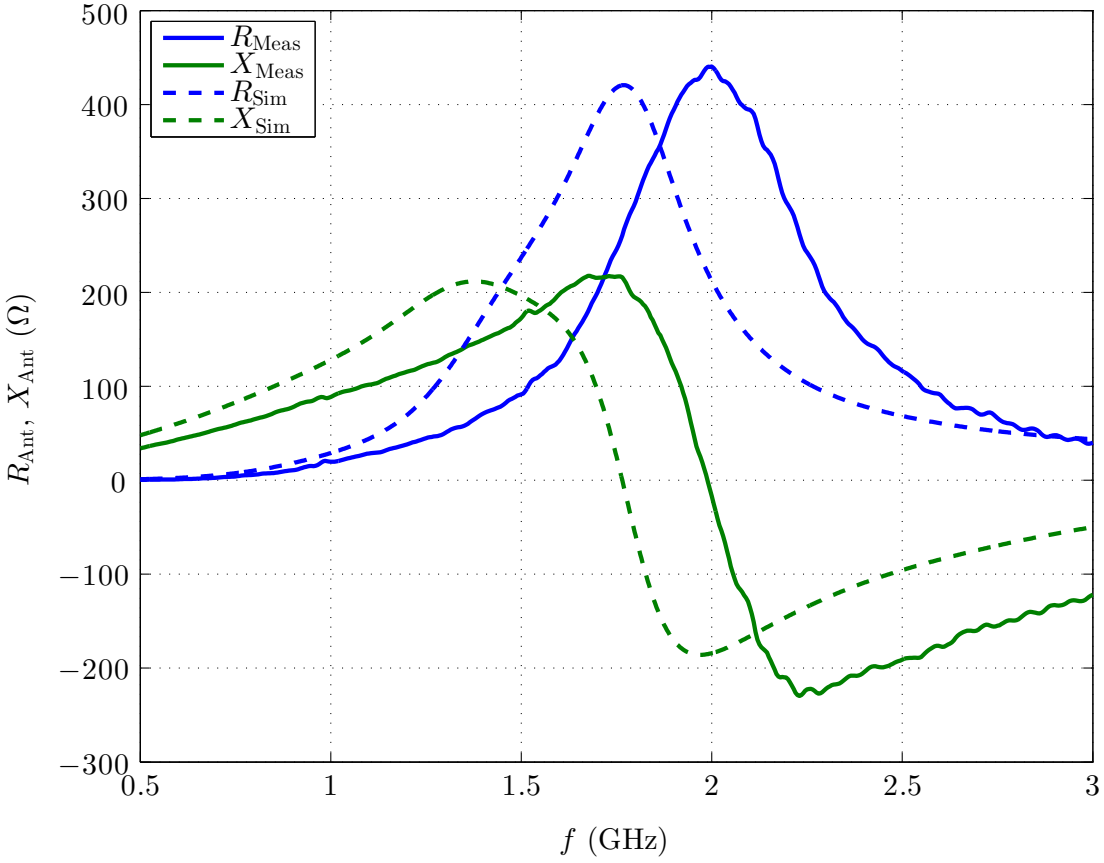

Figure 3.14: Antenna resistance R_{Ant} and reactance X_{Ant} versus frequency f at 5 mm water filling level

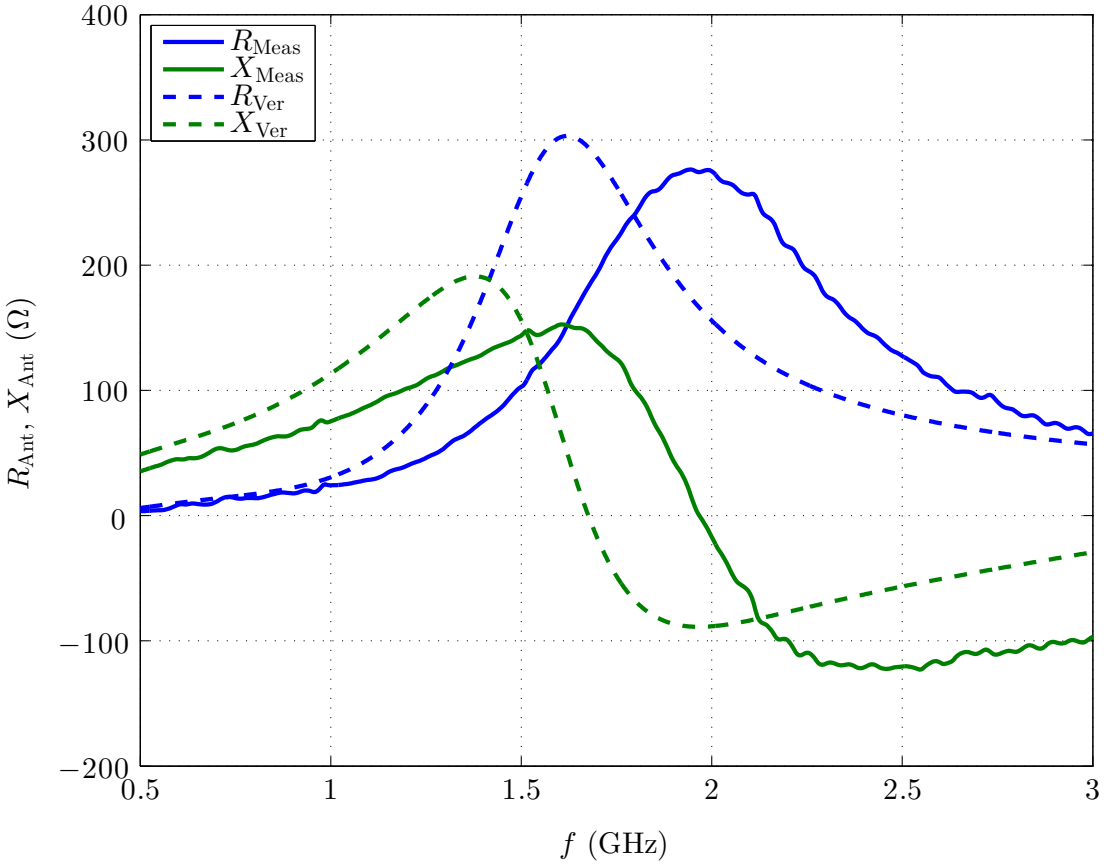

Figure 3.15: Antenna resistance R_{Ant} and reactance X_{Ant} versus frequency f at 40 mm water filling level

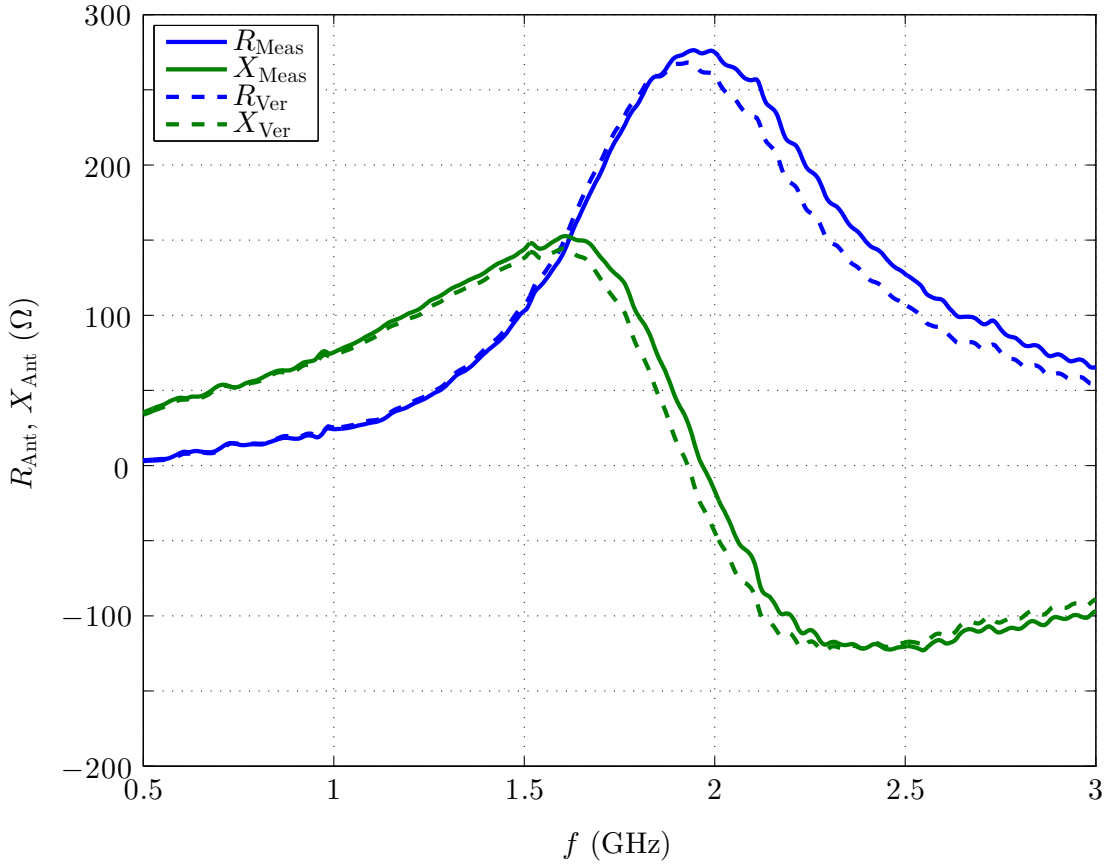

Figure 3.16: Reproducibility measurement: The prototype (R_{Meas}, X_{Meas}) is compared to a second sample (R_{Ver}, X_{Ver}).

Table 3.4 presents the measured antenna impedances Z_{Ant} of the prototype at the three sensing states ($-20\,\text{mm}$, $5\,\text{mm}$, $40\,\text{mm}$) at $f_c = 915\,\text{MHz}$. The table lists also the corresponding parameters, power transmission coefficient τ, modulation efficiency η, and the phase of the absorbing reflection coefficient φ_{Abs}. These parameters lead to a high backscatter transducer efficiency of $\alpha = 0.91$ for an optimized chip absorbing impedance of $Z_{\text{Abs}} = (10.5 - \text{j}74)\,\Omega$. The corresponding constellation diagram can be seen in Figure 3.17.
Both, the measured (see Figure 3.17) and the simulated antenna transducer (see Figure 3.3) lead to good sensor tag performances that is indicated by high backscatter transducer efficiency parameters α. Deviations of measurement and simulation can be observed (compare Table 3.3 and Table 3.4), but the principal behavior as function of the water filling level is the same in simulation and measurement.

Filling level (mm)	Z_{Ant} (Ω)	τ	η	φ_{Abs} ($^\circ$)
$\Delta_1 = -20$	$5.8 + \text{j}71.1$	0.887	0.11	-22
$\Delta_2 = 5$	$11.8 + \text{j}80.7$	0.916	0.17	84
$\Delta_3 = 40$	$18.5 + \text{j}67.8$	0.883	0.35	-129

Table 3.4: Water filling levels and corresponding parameters of the measured antenna transducer prototype for an optimized chip absorbing impedance of $Z_{\text{Abs}} = (10.5 - \text{j}74)\,\Omega$ at 915 MHz: Antenna impedance Z_{Ant}, power transmission coefficient τ, modulation efficiency η, and phase of the absorbing reflection coefficient φ_{Abs}

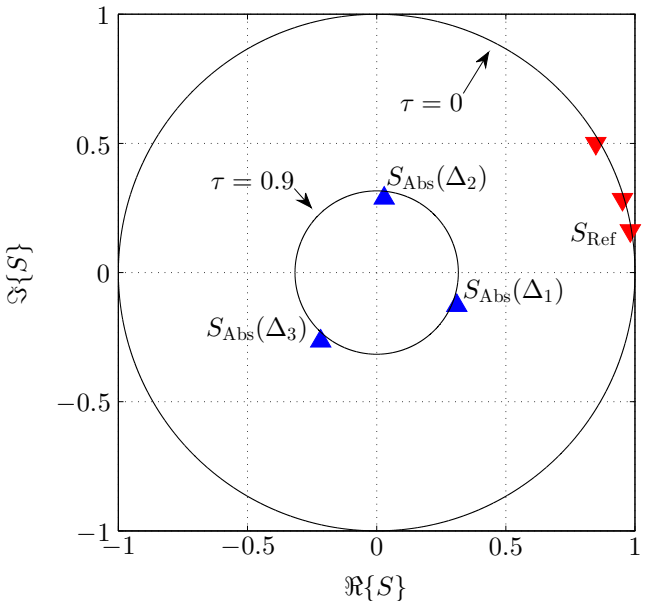

Figure 3.17: Constellation diagram of the measured antenna transducer prototype for an optimized chip absorbing impedance of $Z_{\mathrm{Abs}} = (10.5 - \mathrm{j}74)\,\Omega$ at 915 MHz: This constellation leads to a backscatter transducer efficiency of $\alpha = 0.91$.

4 Conclusions

In passive backscatter RFID systems, the communication between the reader and the tag relies on modulated reflections of the reader RF signal at the tag. Also, the reader supplies the passive tag with RF power. Typically, the tag ID is transmitted to the reader by modulating the amplitude of the reflected signal. This modulation is performed by switching between the tag absorbing and reflecting modes.
This thesis focuses on the design and the development of an antenna transducer to equip a passive RFID tag with sensing capabilities. Such a passive RFID sensor tag provides sensing capabilities without any specific sensor interface and ADCs. A resulting advantage is that an off-the-shelf chip can be used for the passive RFID sensor tag realization.
The novelty of the presented antenna transducer in comparison to previous designs is that the sensor information is mapped to the phase of the reflected signal in the absorbing mode. The big advantage of this concept is that the power transmission to the passive RFID chip stays constant while transmitting the sensing information. With this, a reliable power supply to the tag is guaranteed. Furthermore, a high backscatter modulation efficiency is ensured with such an implementation.
The realized prototype is able to detect three different water filling levels in a can with a high backscatter transducer performance. The deviation of the power transmission coefficient τ from the reference value τ_{ref} does not exceed 2% at each sensing state. Thus, a reliable power supply to the chip is ensured. A high minimum modulation efficiency of $\eta = 0.11$ is achieved, which leads to a reliable tag ID transmission.
An interesting application for the water filling level RFID sensor tag is e.g. to wirelessly monitor the water filling level of a windshield washer system in a car. Also, the developed prototype acts as pioneer for various other prototypes and applications.

Bibliography

[1] J. Landt, "The history of RFID," *Potentials, IEEE*, vol. 24, no. 4, pp. 8–11, 2005 (cit. on p. 1).

[2] J. Grosinger and W. Bösch, "A passive RFID sensor tag antenna transducer," in *Antennas and Propagation (EuCAP), 8th European Conference on*, IEEE, 2014, pp. 3638–3639 (cit. on pp. 1–4, 7, 8, 11–14, 16, 23).

[3] B. Sklar *et al.*, "Rayleigh fading channels in mobile digital communication systems part I: Characterization," in *IEEE Communications Magazine*, Citeseer, 1997 (cit. on p. 1).

[4] P. Nikitin and K. Rao, "Performance limitations of passive UHF RFID systems," in *IEEE Antennas and Propagation Society International Symposium*, vol. 1011, 2006 (cit. on pp. 1, 2).

[5] G. Marrocco *et al.*, "Multiport sensor RFIDs for wireless passive sensing of objects - Basic theory and early results," *Antennas and Propagation, IEEE Transactions on*, vol. 56, no. 8, pp. 2691–2702, 2008 (cit. on p. 1).

[6] J. Grosinger, *Backscatter radio frequency systems and devices for novel wireless sensing applications*. Ph.D. thesis, Vienna University of Technology, 2012 (cit. on pp. 2–9).

[7] P. Nikitin *et al.*, "Power reflection coefficient analysis for complex impedances in RFID tag design," *IEEE Transactions on Microwave Theory and Techniques*, vol. 53, no. 9, pp. 2721–2725, 2005 (cit. on pp. 3, 4).

[8] J. Grosinger and M. Fischer, "Bandwidth issues of UHF RFID transponder antennas for advanced tire monitoring," in *Antennas and Propagation in Wireless Communications (APWC), IEEE-APS Topical Conference on*, 2011, pp. 496–499 (cit. on p. 4).

[9] B. Rembold, "Optimum modulation efficiency and sideband backscatter power response of RFID-tags," *Frequenz*, vol. 63, no. 1-2, pp. 9–13, 2009 (cit. on p. 4).

[10] K. Finkenzeller, *RFID handbook: fundamentals and applications in contactless smart cards, radio frequency identification and near-field communication, third edition*. John Wiley & Sons, Ltd, 2010 (cit. on p. 6).

[11] C. Angerer, *Design and exploration of radio frequency identification systems by rapid prototyping*. Ph.D. thesis, Vienna University of Technology, 2010 (cit. on p. 6).

[12] G. Marrocco and F. Amato, "Self-sensing passive RFID: From theory to tag design and experimentation," in *Microwave Conference, EuMC*, IEEE, 2009, pp. 1–4 (cit. on p. 9).

[13] R. Bhattacharyya *et al.*, "Low-cost, ubiquitous RFID-tag-antenna-based sensing," *Proceedings of the IEEE*, vol. 98, no. 9, pp. 1593–1600, 2010 (cit. on p. 9).

[14] S. Capdevila *et al.*, "Passive RFID based sensing," in *RFID-Technologies and Applications (RFID-TA), IEEE International Conference on*, 2011, pp. 507–512 (cit. on p. 9).

[15] Z. Jiang *et al.*, "RFID tag antenna based wireless sensing method for medical transfusion applications," in *RFID-Technologies and Applications (RFID-TA), IEEE International Conference on*, 2012, pp. 126–130 (cit. on p. 9).

[16] S. Merilampi *et al.*, "Printed passive UHF RFID tags as wearable strain sensors," in *Applied Sciences in Biomedical and Communication Technologies (ISABEL), 3rd International Symposium on*, IEEE, 2010, pp. 1–5 (cit. on p. 10).

[17] C. Occhiuzzi *et al.*, "Passive RFID strain-sensor based on meander-line antennas," *Antennas and Propagation, IEEE Transactions on*, vol. 59, no. 12, pp. 4836–4840, 2011 (cit. on p. 10).

[18] R. Bhattacharyya *et al.*, "Towards tag antenna based sensing - An RFID displacement sensor," in *RFID, IEEE International Conference on*, 2009, pp. 95–102 (cit. on p. 10).

[19] J. Gao *et al.*, "Printed electromagnetic coupler with an embedded moisture sensor for ordinary passive RFID tags," *Electron Device Letters, IEEE*, vol. 32, no. 12, pp. 1767–1769, 2011 (cit. on p. 10).

[20] S. Manzari *et al.*, "Humidity sensing by polymer-loaded UHF RFID antennas," *Sensors Journal, IEEE*, vol. 12, no. 9, pp. 2851–2858, 2012 (cit. on p. 10).

[21] J. Virtanen *et al.*, "Temperature sensor tag for passive UHF RFID systems," in *Sensors Applications Symposium (SAS)*, IEEE, 2011, pp. 312–317 (cit. on p. 10).

[22] Q. Qiao *et al.*, "Read range and sensitivity study of RFID temperature sensors," in *Antennas and Propagation Society International Symposium (APSURSI)*, IEEE, 2012, pp. 1–2 (cit. on p. 10).

[23] A. Babar *et al.*, "Passive UHF RFID tag for heat sensing applications," *Antennas and Propagation, IEEE Transactions on*, vol. 60, no. 9, pp. 4056–4064, 2012 (cit. on p. 10).

[24] S. Caizzone *et al.*, "Multi-chip RFID antenna integrating shape-memory alloys for detection of thermal thresholds," *Antennas and Propagation, IEEE Transactions on*, vol. 59, no. 7, pp. 2488–2494, 2011 (cit. on p. 11).

[25] C. Occhiuzzi *et al.*, "RFID passive gas sensor integrating carbon nanotubes," *Microwave Theory and Techniques, IEEE Transactions on*, vol. 59, no. 10, pp. 2674–2684, 2011 (cit. on p. 11).

[26] ——, "Modeling, design and experimentation of wearable RFID sensor tag," *Antennas and Propagation, IEEE Transactions on*, vol. 58, no. 8, pp. 2490–2498, 2010 (cit. on p. 11).

[27] MATLAB, *version 8.2.0.701 (R2013b)*. Natick, Massachusetts: The MathWorks Inc., 2013 (cit. on p. 16).

[28] ARLON Microwave Materials. (2014). AR1000, [Online]. Available: `https://imageserv11.team-logic.com/mediaLibrary/303/AR1000.pdf` (visited on 10/13/2014) (cit. on p. 23).

[29] Kern GmbH. (2014). Polyethylene high density (PE-HD), [Online]. Available: `http://www.kern-gmbh.de/cgi-bin/riweta.cgi?nr=1411&lng=2` (visited on 10/13/2014) (cit. on p. 23).

[30] CST STUDIO SUITE, *version 2014.03*. Darmstadt, Germany: CST Computer Simulation Technology AG, 2014 (cit. on p. 23).

[31] J. Grosinger *et al.*, "UHF RFID transponder chip and antenna impedance measurements," in *Proc. EURASIP Workshop on RFID*, 2010 (cit. on pp. 27, 30).

[32] RS Components Handelsges.m.b.H. (2014)., [Online]. Available: `http://at.rs-online.com/web/p/hf-und-koax-adapter/7385941/` (visited on 10/23/2014) (cit. on pp. 27, 29).

[33] Rohde & Schwarz GmbH & Co.KG. (2014). R&S ZVA / R&S ZVB / R&S ZVT, Vector Network Analyzers Operating Manual, [Online]. Available: http://cdn.rohde-schwarz.com/pws/dl_downloads/dl_common_library/dl_manuals/gb_1/z/zva_2/ZVA_ZVB_ZVT_Operating_en_24.pdf (visited on 10/10/2014) (cit. on p. 30).